Chemical Engineering Science, Vol. 45, No. 3, pp. 639–650, 1990.
Printed in Great Britain.

0009–2509/90 $3.00 + 0.00

STEAM BUBBLING REGIMES AND DIRECT CONTACT CONDENSATION HEAT TRANSFER IN HIGHLY SUBCOOLED WATER

AYODEJI JEJE, BENJAMIN ASANTE and BRIAN ROSS
Department of Chemical and Petroleum Engineering, The University of Calgary, Alberta, Canada T2N 1N4

(*Received* 12 *September* 1988; *accepted for publication* 3 *July* 1989)

Abstract—Experiments are reported on the growth of vapor liquid interfaces dominated by both inertial and thermal effects. The system involved supplying saturated steam, at steady rates, to a 5 mm diameter nozzle submerged in water at 15–20° C. Discrete bubbles were released at steam injection rates below 1.6 $g\,s^{-1}$ or 2.56 $(10^{-3})\,m^3\,s^{-1}$. Between 1.9 and 6.1 $g\,s^{-1}$ axisymmetric jets periodically evolved from ellipsoidal cavities above the orifice. Continuous two-phase jets from rapid disintegration of the vapor stream were not achieved at rates as high as 6.7 $g\,s^{-1}$ or 6.72 $(10^{-3})\,m^3\,s^{-1}$. In the transition between unstable and continuous jets, the interface evolved alternately to detach large bubbles from axisymmetric jets and small bubbles during "tip streaming" from tapering sinuous jets. At all steam rates, the periods of cavity growth to bubble detachment were less than 3 ms and the maximum cavity volumes were about 400 mm^3. The vapor–liquid boundaries were highly irregular due to spontaneous turbulence. The turbulence and temperature elevation at the boundaries promoted local desorption of gas from the water. The tiny bubbles formed persisted and were convected as discrete but axially dispersing clouds in the plume. Detached vapor bubbles disintegrated and collapsed completely within less than three nozzle diameters from the orifice. Convective heat transfer coefficients at the evolving vapor–liquid interfaces varied with the bubbling regime and with the stage of interface growth, and were as high as 2.4 $MW\,m^{-2}\,K^{-1}$ without the pool of water being agitated.

INTRODUCTION

Sparging of condensable or highly soluble gases into liquids is extensively carried out in the process industry for mass transfer and rapid dispersal of solutes in a liquid, or to achieve high rates of heat transfer through direct contacting of two fluids at different temperatures, with or without phase transformation (Sideman, 1966). The scheme of contacting the fluids is important. Often a high level of turbulence convected in buoyant jets (Abramovich, 1963; Turner, 1973; Chen and Rodi, 1980) is desired within the bulk liquid. Mechanical etching due to rapid implosion of cavities or vapor bubbles near solid surfaces (Benjamin and Ellis, 1966; Plesset and Chapman, 1971; Lauterborn and Bolle, 1975; Plesset and Prosperetti, 1977) may have to be avoided or is desired. A motivation for the study is the possible application of the latter for disintegrating lumps of particulate solids mixed with liquids to produce slurries. Knowledge of the growth process of the vapor–liquid interface and estimates for the range of bubble size produced in subcooled water from saturated steam are important information.

The growth of interfaces on injecting non-condensable gases through submerged orifices, the detachment of bubbles and their rise in liquids have been extensively studied experimentally (see reviews by Kumar and Kuloor, 1970; Clift *et al.*, 1978; Levich, 1962; Wegener and Parlange, 1973) and theoretically (Silberman, 1957; Davidson and Schüler, 1960a, b; Pinczewski, 1981; Tan and Harris, 1986) under isothermal conditions. The primary forces which regulate the growth of cavities at the orifice and the volumes of bubbles released are surface tension, inertia, viscous and form drag, and buoyancy.

When steam is injected into a large pool of cold water, the viscosity of the liquid and the surface tension will not remain constant near or at the surfaces of the cavities which expand to release bubbles. Hence, the growth dynamics of air–water and steam–water interfaces are expected to be different. Three other factors may contribute to the variations. First, since the vapor pressure of steam is higher than the thermodynamic (equilibrium) vapor pressure for cold water, some steam would be condensing at the interface as a bubble expands. That is, the interface is displaced only by a fraction of the vapor stream approaching the surface (Jeje and Ross, 1988). The residual velocity for the vapor depends on the rate at which heat is convected away from the liquid side of the boundary. Secondly, high energy and mass transfer rates promote spontaneous interfacial turbulence and oscillations (Gardner *et al.*, 1955). The instabilities, in turn, affect the growth dynamics for the interface. Spontaneous convection occurs at a free surface when the Rayleigh number, Ra $(g\alpha\Delta T d^3/\kappa\nu)$, exceeds 657.5 (Chandrasekhar, 1961; Krishnamurti, 1970; Koschmieder and Pallas, 1974; Mollendorf *et al.*, 1984). Significant turbulence in the ambient fluid promotes the onset of the convection (Foster, 1971). These conditions are met when saturated steam contacts cold water. In the definition for Ra, ΔT is the temperature difference across a layer of characteristic thickness d and κ is the thermal diffusivity $(k/\rho C_p)$.

A characteristic thickness of $(\kappa t)^{1/2}$ (Howard, 1963)

leads to convective motions starting after about 0.8 s when ΔT is 80°C. External disturbances strongly reduce the lag time for onset of hydrodynamic instability to a period much shorter than 0.074 s. The latter was estimated from Foster's (1971) expression $14.0(\nu/\alpha g\dot{Q}_k)^{1/2}$. In the relationship, the "kinematic" heat flux ($\dot{Q}_k$) was evaluated from $h\Delta T/\rho C_p$ and the heat transfer coefficient (h) was 7.6 (10^4) W m^{-2} K^{-1} or the lower bound of data reported by Bankoff and Mason (1962). The foregoing shows that turbulent convective motions would rapidly evolve at the vapor–liquid boundary. Onset periods would be shorter still for higher ΔT and h values. This was confirmed in photographic evidence to be presented.

The third factor is that an entrainment flow would be established as heated water rose in the buoyant field near the orifice (Chen and Rodi, 1980). The buoyant jet formed would have features both different from and in common with isothermal, two-phase plumes (Kobus, 1968; Milgram, 1983) and steady, non-isothermal, single-phase jets (Turner, 1973). Water may be displaced with periodic puff motions (Richards, 1965), or the flow may be toroidal (Zauner, 1985). Such unsteady motions may affect the dynamics of bubble growth. When the entrainment flow is significant, at high steam injection rates, the shape of bubbles may become prolate and taper to discharge small bubbles at the apices, a phenomenon called "tip streaming" in a circular hyperbolic field (Taylor, 1934; Rumscheidt and Mason, 1961; Rallison, 1984).

It is expected that, like the air–water system, different bubbling regimes will be exhibited by the steam–water system. However, the conditions and dynamic characteristics of the interfaces would show variations. In this study, the growth rates of cavities at the orifice, frequencies of bubble release, convective heat transfer coefficients for interfaces confined within the nozzle and above the orifice, and the displacement velocities of the vapor–liquid interface into and out of the nozzle were examined.

EXPERIMENTS

The equipment and procedures for the experiments were essentially the same as previously described (Jeje and Ross, 1988), except that the 5 mm diameter nozzles were constructed of plexiglass or quartz glass for transparency. Of two nozzles, the length was 15 mm for one and the hole expanded abruptly into a 16 mm concentric tube. The pore for the other nozzle was 10 mm long and a converging insert with parabolic outline was placed between the supply tube and the nozzle hole. Both nozzles were tested to determine whether the small changes in pressure due to contraction of the channel affected bubble formation dynamics. No significant differences were found. Temperatures and pressures were monitored at the steam side of the nozzle. Within the pool, particularly in the buoyant jet, temperatures were determined with thermocouples with dynamic responses higher than 5.5°C ms^{-1} and the signals recorded on magnetic tapes using a Hewlett–Packard (HP) Structural Dynamics Analyzer. Signals from a Geosource hydrophone immersed in the pool to determine pressure wave patterns emanating from the nozzle region were also recorded with the HP Analyzer.

Photographic patterns of the buoyant jet and the evolution of bubble growth, detachment and collapse were recorded using different optical arrangements. Still photographs, with illumination duration of 1–50 μs from a spark arc source and electronic flashes, were obtained in the preliminary part of the study. High speed movie photographs were taken with a Hycam (Redlake Inc.) camera operated at 3000 and 5000 frames per second (fps) with front illumination using a mercury lamp. A Dynafax (Beckman–Whitley) camera operated at 25,000 fps (1 μs exposures) was used with a basic Schlieren optical system for recording high resolution silhouettes of bubble growth and collapse and the convective patterns around the nozzle.

The rates of steam injection for the experiments were varied between 0.9 $\pm$ 0.05 and 6.7 $\pm$ 0.02 g s^{-1}, i.e. nominal vapor input velocities through the 5 mm nozzle of 83.5–342 m s^{-1} (< sonic velocity of 475.7 m s^{-1}). The corresponding saturation temperatures (T_s) were 97.5 and 116.2°C. At steam rates greater than about 1.5 g s^{-1} (T_s = 101°C), negligible backflooding into the nozzle holder occurred since liquid retraction was most often less than 4 mm. The vapor flow, in converging into the nozzle from a 16 mm tube upstream, was essentially isenthalpic. Although a very small temperature decrease accompanied the change in pressure, a slight superheat was associated with the volumetric expansion. Consequently, droplets of liquid were not formed within the nozzle or at the exit. The entire energy content of the steam was directly transferred to the water in the pool. The bulk liquid temperatures were maintained at 16.5 $\pm$ 0.5°C and the column of water was 0.9 m high for all the runs.

RESULTS AND DISCUSSION

Pressure wave pulses

The mean frequencies of pressure wave propagation from the nozzle over the range of steam supply rates investigated are presented in Fig. 1. At steam rates lower than 1.6 g s^{-1}, the dominant frequency for eruption of bubbles was essentially constant at approximately 16 Hz. This was established by averaging 10 consecutive scans for fixed Data Analyzer bandwidths in the 50–800 Hz range. Eruption frequencies were, however, not the same as bubble release frequencies. Photographic records show that at a steam input rate of 1.45 g s^{-1}, an average of four bubbles were released per eruption. Apparently only the first or primary bubble generated a measurable pressure wave. Between 1.6 and 1.9 g s^{-1}, the pressure wave patterns were erratic and multiple peaks ranging from 16 to 750 Hz were recorded. The peaks were not harmonics of the lowest significant frequency and for these steam rates, transition between two bubbling regimes seemed to occur. In the 1.9–6.1 g s^{-1} steam

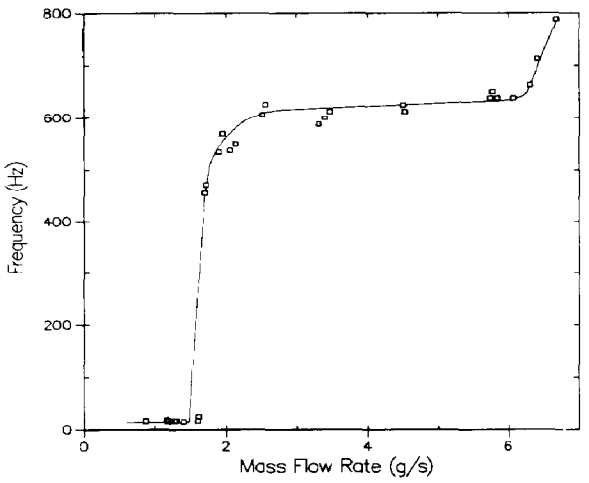

Fig. 1. Frequencies of vapour bubble eruptions for saturated steam at 97–117°C flowing through a 5 mm diameter nozzle in water at 16.5 ± 0.5°C.

input rate range, a dominant frequency which increased slowly from 600 to 650 Hz was re-established. For the range, photographic records show that each bubble detachment cycle was correlated to the pressure pulse frequency. For a steam supply rate slightly greater than 6.5 $g\,s^{-1}$, multiple frequency peaks were again observed in a transition zone between unstable and continuous jet regimes. The dominant frequency ranged between 700 and 800 Hz. The regimes, as deduced from the frequency data, are single bubbles, unstable jets and two transition zones. A steady, continuous jet was not observed within the range of steam rates investigated. Photographic evidence on the regimes of steam bubbling in subcooled water, and dynamic characteristics of the growth, detachment and collapse of the interfaces are presented in the following.

Regimes of bubbling

Discrete bubble regime. Discrete bubbles were released intermittently at constant steam supply rates less than 1.6 $g\,s^{-1}$ or nozzle velocities below 125 $m\,s^{-1}$. The corresponding upper bound for observing discrete bubbles of air form in water was about 0.8 $m\,s^{-1}$ through the same orifice. Although the rates of displacement of the vapor–liquid boundary were about an order of magnitude higher than for the air–water system in similar bubbling regimes, a ratio of more than 150 would have been suggested from the figures above. Such large differences in gas/vapor injection rates confirm the significant importance of condensation of vapor at the bubble surface.

Data for the positions of the apices of vapor–liquid interfaces versus time for seven consecutive eruption cycles, at a steam injection rate of 1.45 ± 0.05 $g\,s^{-1}$, are presented in Fig. 3(a). These were derived from projection of high speed pictures [as in Fig. 2(a) at 3250 fps] at a screen. The data in Fig. 3(a) show that the dynamics for forming consecutive bubbles were different. Starting from when a bubble had just been released, the interface may retract as deep as 12 mm into the nozzle (curve 1). The surface often oscillated around a mean position while retracted deep into the nozzle pore. The interface was then displaced outward (curve 2) until a bubble was pinched. Frequently, a detached bubble was not significantly displaced away from the orifice while it collapsed and a subsequent cavity growth was initiated at the orifice. Under this condition, the evolving cavity was depressed along the nozzle axis to form a bowl, from the edge of which two or three small bubbles were released. The next cycle is represented by curves 3 and 4. The retraction was shallower and the bubble released was smaller. A third and possibly fourth cycle involved smaller bubbles being released before cycles 1 and 2 were approximately repeated. That is, the periods for forming consecutive bubbles were not constant. This behavior is characteristic for a chaotic system (Shaw, 1984). An incomplete return or Poincaré map for the events is shown in Fig. 3(b). The curves describe the trajectories of the interface. Plots for a large number of consecutive eruptions show that the trajectories form a band with at least three nested loops. Oscillations at the interface were sufficiently vigorous [Fig. 2(a)] that an exposure of 1/8125 s could not freeze the motion. Moreover, with front illumination, the outlines of the interfaces were partially obscured by tiny gas bubbles desorbed from the water at the interface.

A sequence of photographs of the vapour–liquid boundary at the orifice, taken with the Dynafax and the Schlieren optical set-up at 1 μs exposure, is presented in Fig. 2(b). These show that, during growth above the nozzle, cavities were significantly distorted from a spherical shape. The configuration of the apex may be attributed to a potential core flow of vapor through the nozzle which had not yet been dissipated. A bubble was initially flattened as an oblate spheroid with an irregular surface supported on a short vapor column with the same diameter as the orifice. The evolution of both irregularities on the surface and the Schlieren patterns for warm water around the interface suggest that interfacial turbulence must have developed in time scales less than 0.5 ms. At later stages, the cavity became more prolate in evolving towards releasing a bubble. Detached bubbles were nearly spherical but the collapse was not radially symmetric. The 0.1–0.3 mm diameter gas bubbles desorbed from water formed only while the cavity expanded or detached bubbles oscillated and collapsed above the orifice. They were densely populated and were convected in the buoyant jet as intermittent clouds. High speed and still Schlieren photographs of the growing cavity taken at 2–5X magnification suggest that these bubbles originated at the vapour–liquid interface as gas released to the vapor side of the boundary was enveloped and discharged back into the liquid. The creation took less than 40 μs. Homogeneous nucleation of the bubbles did not appear to have occurred even within the boundary layer around the

vapor cavity in the water, which undoubtedly had a large population of microscopic solid particles. Thus, an elevated temperature, high local turbulence and interfacial perturbations were required for their formation.

Figures 4 and 5 show the volumes of the cavity and the areas of the vapour–liquid interface which were estimated from photographs versus time during axisymmetric growth above the orifice. To estimate these parameters, the projected outlines of the cavity above the orifice were digitized in the x–y coordinates. By rotating the half curves around the nozzle axis, two volumes and areas were obtained by numerical integration for nearly axisymmetric cavities. When the cavities deviated significantly from axisymmetry, for higher accuracy, the outlines were divided into horizontal parts before volumes and areas of revolution were calculated. Arithmetic average values of the two results were obtained and are presented in the figures. From the data in Figs 3(b) (instantaneous residual velocity of interface), 4 (volumetric rate of cavity expansion) and 5 (rate of increase in interfacial area), the surface-average heat transfer coefficient (h) may be estimated as a function of time at the liquid side of the

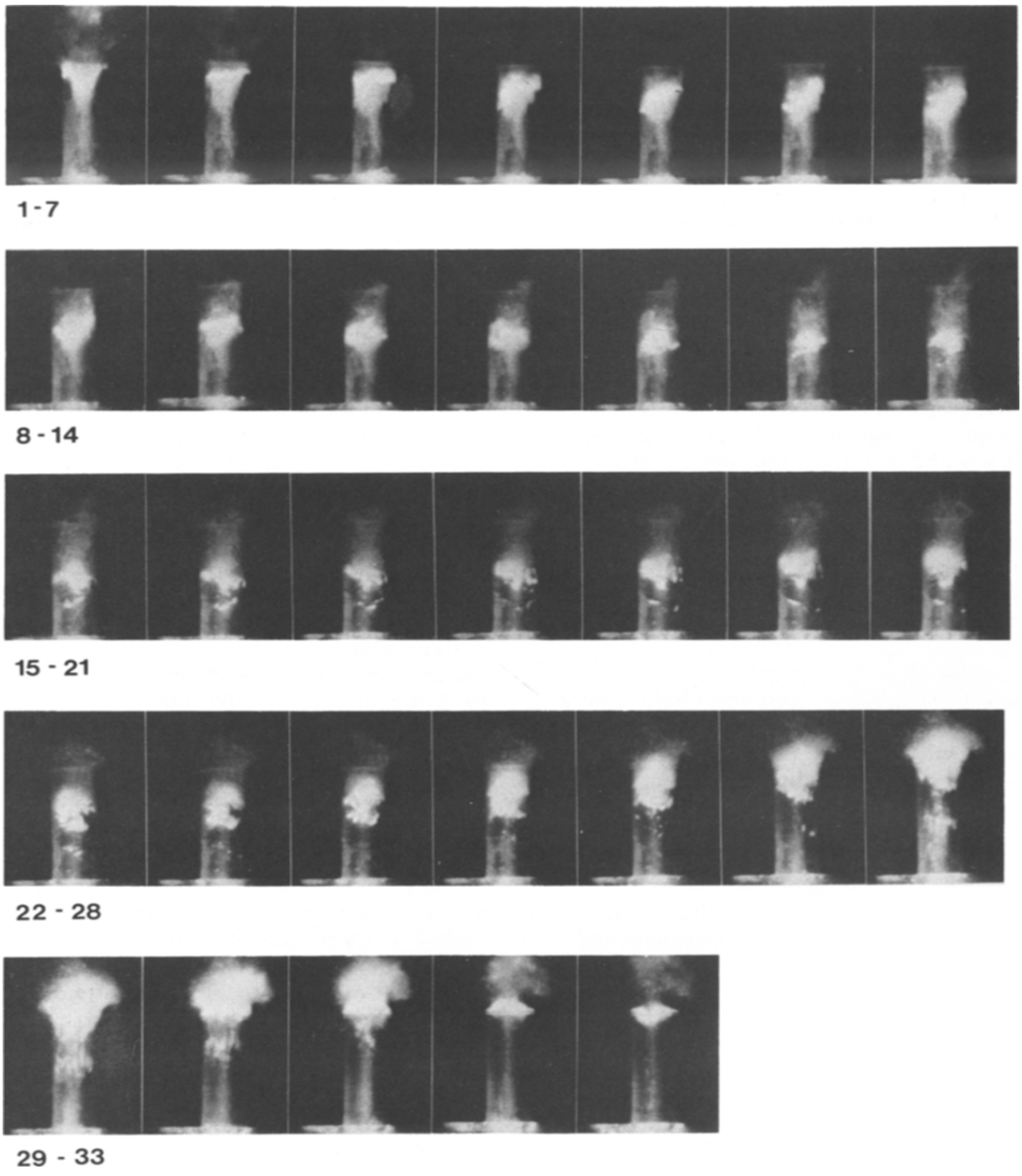

Fig. 2. (a).

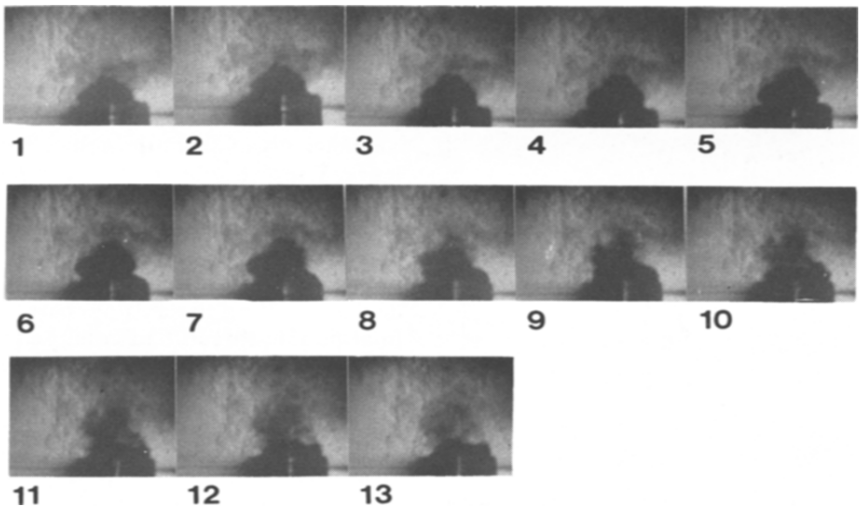

Fig. 2. (b).

Fig. 2. Photographic sequences of interface displacement within the nozzle pore and outside the orifice. (a) Pictures taken at 3250 fps (0.123 ms exposure) with front illumination at a steam rate of 1.45 $g\,s^{-1}$ (308 μs between frames). Retraction of the interface into the nozzle pore occurred in the sequence 1–15, ascent in 16–26 and cavity growth to bubble detachment in sequence 27–31. (b) Pictures taken at 25,000 fps (1 μs exposure) with Schlieren optical set-up for viewing the region above the orifice at a steam rate of 1.45 $g\,s^{-1}$ (80 μs intervals between plates).

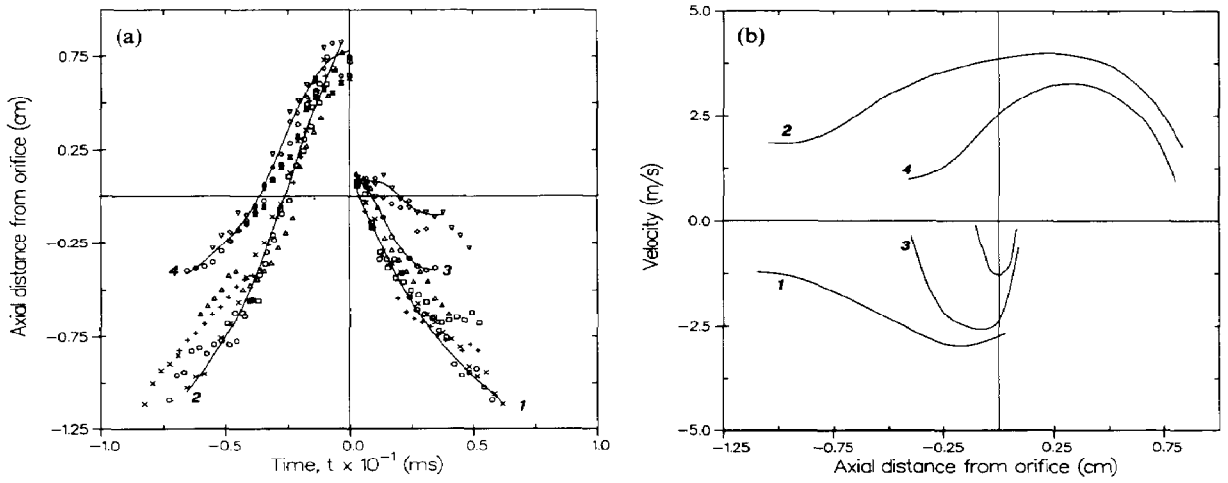

Fig. 3. (a) Locations of vapor–liquid interface within and outside a 5 mm diameter nozzle for seven eruption cycles at a steam rate of 1.45 $g\,s^{-1}$. Retraction of interfaces and ascent to release primary bubbles are curves 1 and 2 respectively. Shallow withdrawals of interface for secondary bubble formation are for the other data on the right of the ordinate (e.g. curve 3) and upwards interface displacements to form the bubbles are data set 4. The instant of bubble detachments has been chosen as time zero. (b) Velocities of displacement of the apices of the vapour–liquid boundaries within and outside the nozzle as calculated from the solid curves in Fig. 3a. The conditions and the sequence numbers are the same as for (a).

interface. The expression relating the parameters is:

$$\bar{h}(t) = \frac{\Lambda \Delta H_v}{A(t)(T_{sat} - T_b)} \qquad (1)$$

where Λ equals $[\dot{m} - \rho_v \dot{V}(t)]$ for bubble growth above the orifice. When the interface is located within the pore, the rate of condensation at the interface is given by:

$$\Lambda = \pi r_0^2 [(u_0 - u_1)\rho_v]. \qquad (2)$$

In eq. (1), $\dot{m}$ is the mass input rate of steam, $\dot{V}(t)$ is the rate of change of the volume of the cavity above the orifice, ρ_v is vapor density, ΔH_v is the latent heat of vaporization, $A(t)$ is the surface area of the vapour–liquid interface, and T_{sat} and T_b are the saturation temperature and the bulk liquid temperature respectively. While the interface is confined within the nozzle pore, Λ is given by eq. (2) where u_0 and u_1 are the velocity for the vapor through the nozzle (i.e.

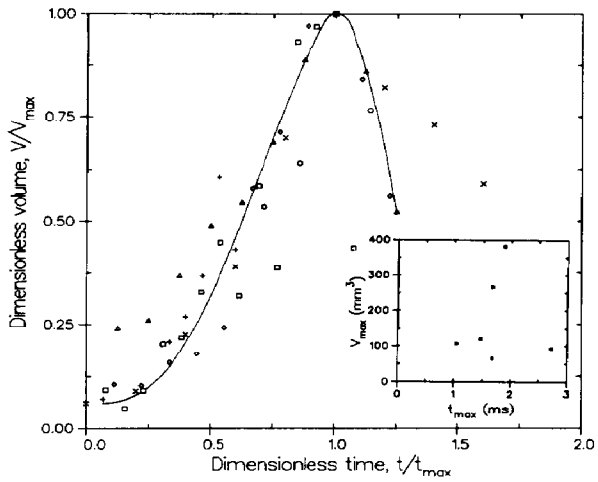

Fig. 4. Volumes of seven vapor cavities above the orifice as functions of time on a normalized basis. V_{max} and t_{max} (insert) are the maximum volumes and corresponding period of evolution of the cavity.

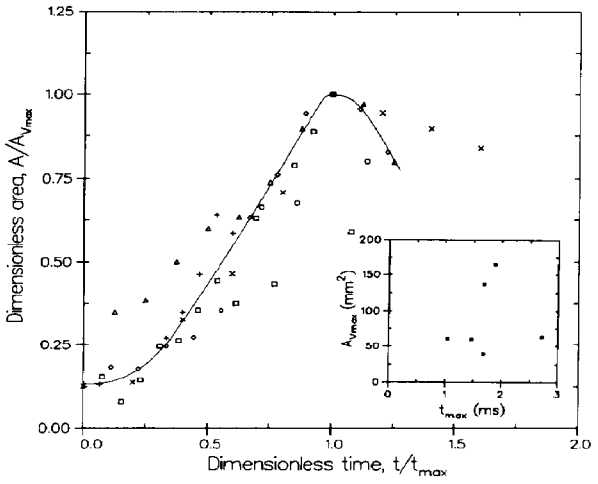

Fig. 5. Areas of vapor–liquid boundary for cavities presented in Fig. 4 on a normalized basis. The values for $A_{V_{max}}$ (insert) are interface areas for cavities at the instances when the maximum volumes were achieved.

before reaching the interface) and the spatially-averaged displacement rate of the interface respectively.

Bubble detachment occurred very rapidly and inertia and buoyancy forces seemed to dominate the growth phase. As is evident in Fig. 2(b) and the cavity volume data in Fig. 4, the bubble volume had actually begun to decrease by the time a constriction developed rapidly near the base of the cavity. Schlieren patterns around the evolving bubbles indicated that unheated water penetrated to the interface in the region of constriction. The growth patterns for seven cavities above the orifice are presented in Fig. 4 on a non-dimensionalized basis. The narrow scatter of the data around a mean curve indicates that the patterns of volumetric expansion were similar for the different cavity sizes. After the detachment and disintegration of each bubble, the temperature distribution in the radial direction within the buoyant jet is suggested to be nearly uniform at about two nozzle diameters away from the orifice because of the turbulence. Vapor bubble remnants could still exist in this zone, primarily along the nozzle axis. Within five nozzle diameters, the temperature pattern had evolved into a Gaussian profile with a spike along the nozzle axis (Jeje and Ross, 1988). The temperature deviation along the axis appears to reflect where the final bubble thread had collapsed.

Transition to unstable jet regime. Transition between the discrete bubble and the jet regimes occurred for steam rates between 1.6 and 1.9 $g\,s^{-1}$. Water did not retract into the nozzle between eruptions. For relatively long periods, the interface fluctuated around a nearly flat profile above the orifice and a circular rim sometimes extended beyond the nozzle opening. As is shown in the sequence in Fig. 6 for a steam supply rate of $1.61 \pm 0.02\,g\,s^{-1}$, the interface pushed outwards approximately once every 7 ms through a distance less than $0.4\,d_0$ to produce a bubble from a cap with an oblate spheroidal outline. This bubble, pinched from a cavity which evolved in 2.5–3 ms, hardly moved away from the remnant interface while it disintegrated and/or collapsed, most rapidly from the sides. The interface was always highly agitated and produced tiny bubbles of air from the un-degassed water. Such an interface may serve as the source for a pure thermal plume (Chen and Rodi, 1980). The entrainment flows were apparently sufficient to convect away all the latent energy supplied by the steam from the quasi-stationary boundary.

Unstable jet regime. For vapor supply rates of between 1.9 and 6.1 $g\,s^{-1}$, nearly axisymmetric jets were formed periodically in the subcooled water. The patterns of jet evolution at the lower end of the range are slightly different from those for the upper range as the sequence in Figs 7 and 8 show. At a steam supply rate of 3.33 $g\,s^{-1}$ (Fig. 7), the meniscus was an oblate ellipsoid on the orifice at the start of a cycle. The preceding bubble released had almost completely disintegrated and collapsed at about two nozzle diameters away. The oblate form was retained as the interface pushed out and spread laterally away from the orifice. Schlieren patterns of upward flow of warm water were observed mostly at the top of the interface. As the growth continued, the central portion of the top bulged out to deform the surface. The cavity thereafter elongated rapidly with one or two regions of constriction on the cylindrical side while the diameter along the jet continued to decrease. One or two bubbles may eventually be released. When a relatively large bubble was pinched, ambient water appeared to flow towards the core of the bubble from below and the anterior end of the bubble retracted to form a toroidal bubble ring. For a steam supply rate of 5.40 $g\,s^{-1}$ (Fig. 8), lateral spreading of the vapor–liquid interface was not

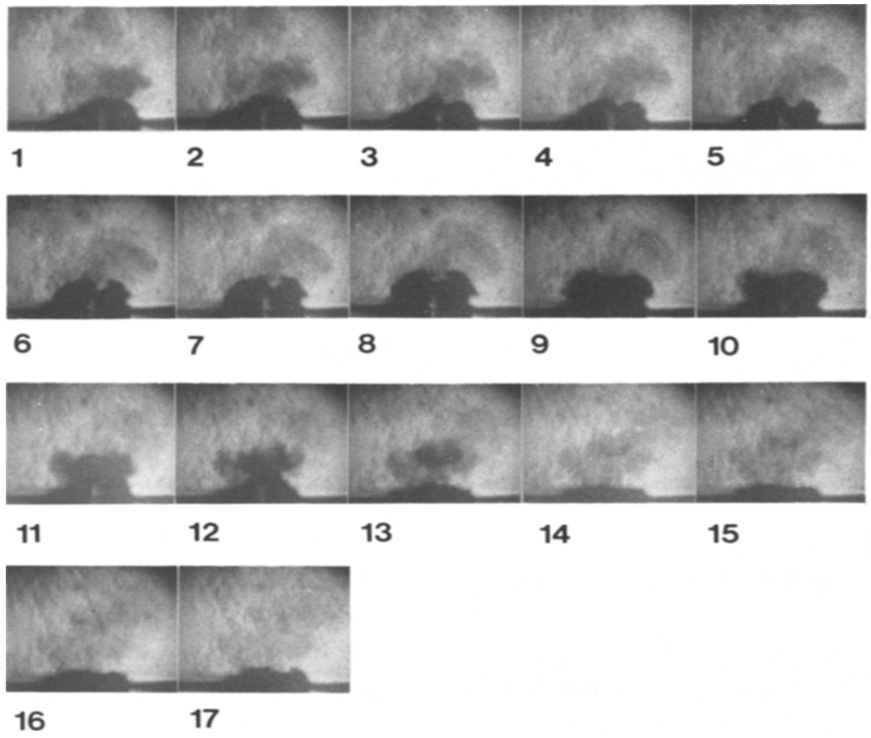

Fig. 6. Photographic sequence of cavity growth in the first trasition zone above the orifice for a steam supply rate of 1.61 $g\,s^{-1}$. Pictures were taken at 25,000 fps (1 μs exposure) and the interval between plates is 160 μs. The sequence 3–13 shows a growth of the cavity to form a bubble. Between 4 and 5 ms elapsed before another such eruption occurred.

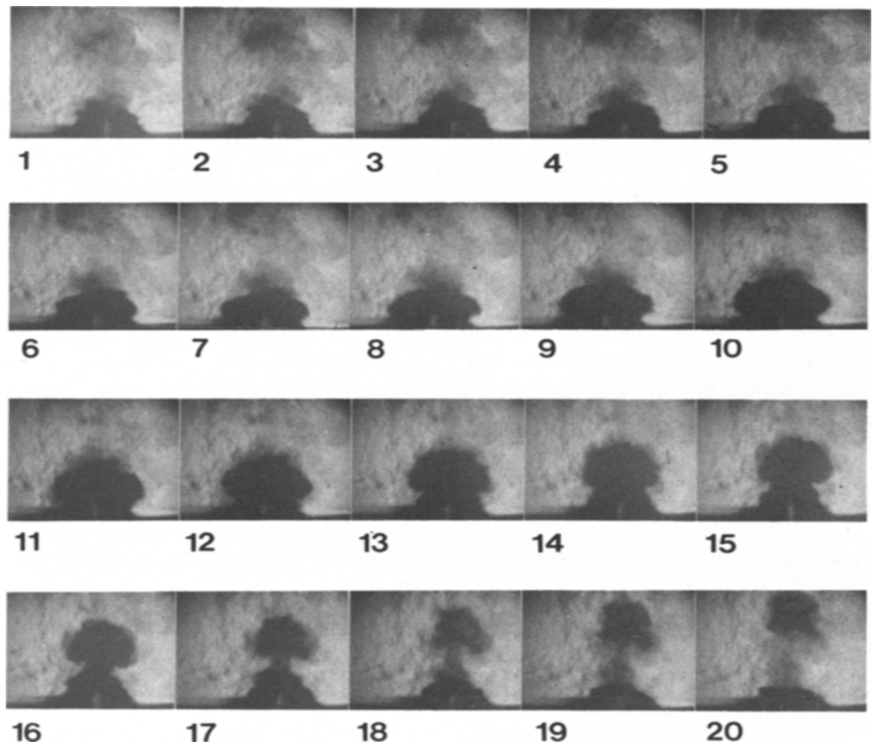

Fig. 7. Photographic sequence of axisymmetric cavity growth and bubble formation in the unstable jet regime at a steam supply rate of 3.33 $g\,s^{-1}$. The interval between plates is 80 μs.

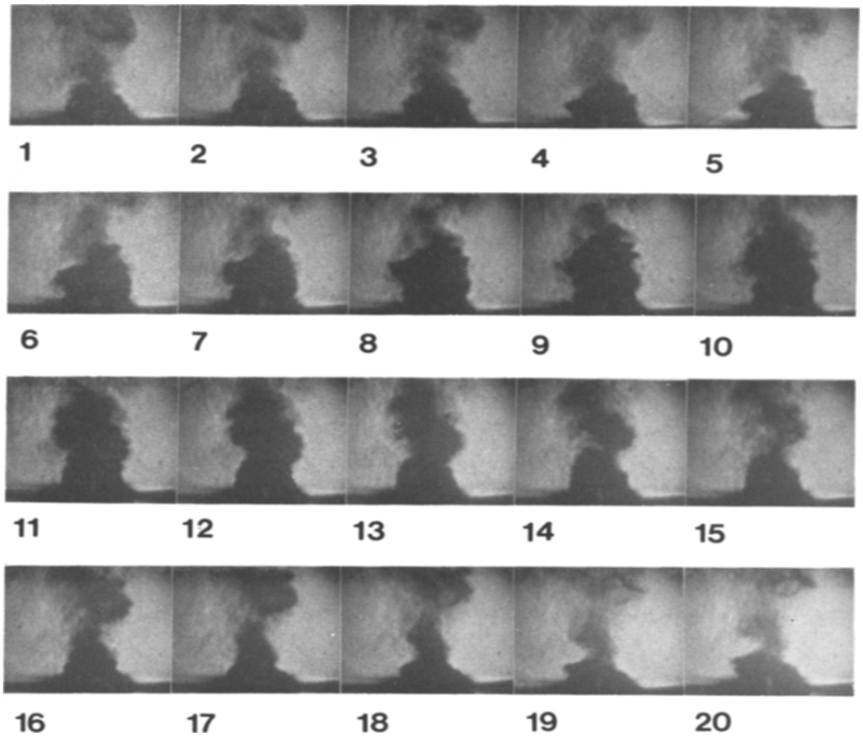

Fig. 8. Photographic sequence of axisymmetric cavity growth in the unstable jet regime for a steam supply rate of 5.40 $g\,s^{-1}$. The vapor–liquid boundaries were highly irregular and bubbles released were distorted significantly from spherical shape. The cavity shapes were mostly prolate. The interval between plates is 80 μs.

as pronounced and the region of constriction was displaced further downstream from the orifice. Relatively large and irregular shaped bubbles were released. Typically, one bubble was released per eruption and ring vortices were more frequently formed from a secondary bubble. As is apparent in both Figs 7 and 8, the vapor–liquid interfaces were highly turbulent throughout an eruption cycle. The periods of growth to detachment and recovery to the initiation of other cycles were between 1 and 2 ms.

Estimates of the volumes of the vapor cavity above the orifice and the vapor–liquid interface areas versus time were determined from photographs using the procedures outlined earlier for a steam supply rate of 3.41 $g\,s^{-1}$ ($T_s = 104.2°C$). The corresponding mean nozzle velocity was 253.7 $m\,s^{-1}$. Because the dynamics for consecutive bubble growth and the final volumes attained at detachment were not identical, the volumes and areas were non-dimensionalized and plotted. The curves were similar to those in Figs 4 and 5 with the following differences. The value for V/V_{max} at $t = 0$ was higher at ≈ 0.18 than in Fig. 4. The maximum cavity volumes also varied between 125 and 150 mm^3. These volumes are significantly smaller than for air bubbles at similar volumetric supply rates of 4.98 $(10^{-3})\ m^3\,s^{-1}$ for a constant flow system (Clift *et al.*, 1978, Fig. 12.2). The bubble volume range, assuming all the cavity was detached, would correspond to an air supply rate of about 5 $(10^{-6})\ m^3\,s^{-1}$. The frequency of release was, however, about 35 times higher and the bubbling regimes were different. The non-dimensionalized areas of the interface versus time, plotted as in Fig. 5, increased to a maximum of ~ 1.12 at $t/t_{max} = 1.2$. That is, the area increased even after the cavity had started to contract as a result of elongation of the bubble. Heat transfer and condensation rates were hence enhanced up to and after the release of bubbles.

Transition to continuous two-phase jet regime. Nearly abruptly at a steam rate of about 6.1 $g\,s^{-1}$, a transition between the unstable and the continuous jet regimes was attained. The intensity of the sound waves emanating from the nozzle decreased and cavities which rapidly varied in length between one and two nozzle diameters were observed attached to the orifice. In the sequence shown in Fig. 9, the jet was almost cylindrical and the aspect ratio (length/diameter) was nearly unity at the beginning of cycle, i.e. shortly after one or two bubbles had been released. The jet elongated first in the axisymmetric mode to release a bubble. The remnant at the orifice exhibited a sinuous profile which tapered to a point at a distance of about two nozzle diameters. "Tip streaming" of small vapor bubbles occurred at the sharp apex. This was often followed by the release of another large

bubble before the original configuration was re-established. The surfaces of the cavity and bubbles were always highly irregular.

Cavity volumes and convective heat transfer coefficients

In the foregoing, the growth of vapor–liquid interfaces, formation of bubbles and their collapse soon after release were described. The range of conditions examined included when backflooding occurred into the nozzle (the pore of which was sufficiently long to preclude weeping into the chamber below) through incipient disintegration of the vapor stream at the nozzle to form a continuous two-phase jet of small bubbles dispersed in cold water.

The formation of vapor bubbles differed significantly from the air–water system in many respects. Although similar regimes were exhibited, the modes of bubble release were different. In the discrete bubble regimes for the air–water system, the growth of bubbles started after a smooth-surfaced spherical cavity had established itself at the orifice. At low flow rates of less than 3 $(10^{-4})\,m^3\,s^{-1}$ through orifices of various sizes (see Kumar and Kuloor, 1970, Fig. 9), bubble volumes were as large as $10^{-5}\,m^3$ and the growth periods were in the 30–70 ms range (Tan and Harris, 1986). The volumes of bubbles formed from the cavity, with the assumptions that the volumes of the remnant were negligible and gas flow rates were high enough for surface tension forces to be negligible (Kumar and Kuloor, 1970; Davidson and Schüler, 1960a,b; van Krevelen and Hoftijzer, 1950), were derived from

$$V_b = \phi(Q^2/g)^{5/3} \qquad (3)$$

where ϕ varied from 0.976 (for the two state process) to 1.722 which was empirically obtained by van Krevelen and Hoftijzer (1950).

An application of eq. (3) for the steam–water system would be inadequate since cavities and bubbles of different volumes were formed at a constant steam supply rate. The variations in volumes are attributed to changes in the intensities of local turbulence and therefore heat transfer rates around the interfaces. In the discrete bubble regime, primary bubbles erupted into a relatively calm environment at intervals of 60–70 ms. The volumes detached were larger than for bubbles formed in multiple eruptions into the liquid zone where previous bubbles had recently collapsed. Even though the ambient liquid temperature near the orifice would be higher for the latter, the elevation in local temperature may not have been large because of dilution caused by liquid entrainment (Jeje and Ross, 1988). It is also important to note that, as shown in Fig. 4 (insert), the volumes of the cavities at the end of the expansion phase were higher than during the detachment phase and the volume of bubbles detached would depend on the relative rates of cavity collapse and bubble pinching. The maximum cavity volumes varied between 5 and 40 $(10^{-8})\,m^3$. Bubble volumes at detachment appeared to be proportional to the maximum cavity volumes in the single bubble and unstable jet regimes. Bubbles formed at higher steam rates were smaller than the maximum achieved in the single bubble regime as jets projected further into the cooler zones of the buoyant jet. Such bubbles were also detached where entrainment flows were more developed away from the nozzle plate and the turbulence in the ambient water more pronounced.

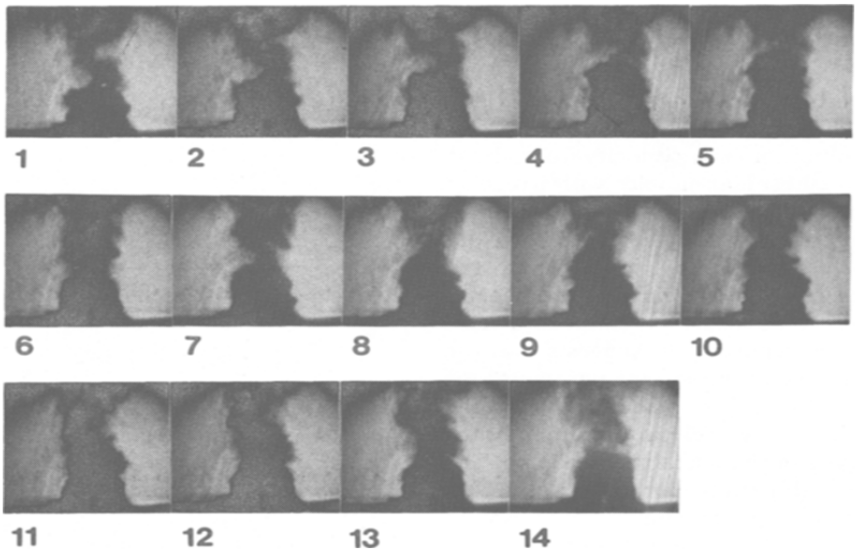

Fig. 9. Photographic sequence of interface growth in the transition region between unstable and continuous two-phase jet regimes. The steam rate was $6.65\,g\,s^{-1}$ and the interval between plates is 80 μs. The interface evolved in the axisymmetric mode in sequence 1–7. The remnant interface was tapered and sinuous in plates 8–13.

The periods of cavity growth were very short, less than 3 ms, compared to bubble formation times for the air–water system. The supply rates of steam through the nozzle at velocities as high as 125 $m\,s^{-1}$ were also considerably higher than for air (up to 5 $m\,s^{-1}$) to observe the same discrete bubble regime. Variations in the displacement velocity with time (or position inside and outside the nozzle pore) in the single bubble regime also indicated that condensation rates of steam at the interface changed with the contact time between the vapor and fresh or unheated liquid.

At low steam supply rates, the interfacial areas of the cavities (Fig. 5) attained maxima when the volumes were highest. This is consistent with photographic observations that during expansion and subsequent collapse of the cavity just prior to bubble release, the final shapes of the cavities were essentially preserved. This suggests that the cavity projected into the liquid transferred heat at high rates from all parts of the surface as if in a uniformly turbulent or homogeneous environment. The frequency of single bubble release (from photographic evidence) was, on a time-averaged basis, about 64 Hz. Primary eruptions occurred at 16 Hz as shown in Fig. 1 for a subcooling of up to 85°C. These are much lower than the 2500 Hz reported by Bankoff and Mason (1962) at low steam injection rates through a 0.5 mm diameter nozzle in a metallic plate. Backflooding may be expected to be minimal or absent in their experimental set-up for saturated steam rates of 6.7 (10^{-3})–1.67 $(10^{-2})\,g\,s^{-1}$. The frequency of eruptions reported in this study are comparable to bubble formation rates reported by Grassman and Wyss (1962).

In the unstable jet regime, the range of volumes achieved by the cavities varied less significantly than for the single bubble regime (Fig. 4, insert) but the frequency of bubble release was an order of magnitude higher. The frequencies of bubble release (600–700 Hz, see Fig. 1) at the 5 mm nozzle were lower than reported by Bankoff and Mason (1962) for steam injection through a 1.73 mm diameter nozzle at 720 Hz. A maximum nozzle velocity of about 17.8 $m\,s^{-1}$ at which ellipsoidal bubbles with irregular surfaces were formed in water with a subcooling of about 50°C were reported by the authors. The velocities obtained were significantly lower than the 125–342 $m\,s^{-1}$ required for the 5 mm diameter nozzle in order for bubbles to be formed at similar frequencies in an unstable jet regime. This suggests that the nozzle diameter may be an important parameter for all the regimes of bubbling. The smaller cavities in the single regime, in this study, were approximately the same size as obtained in the unstable jet regime. The similarity in the growth patterns for cavities of different volumes and the fact that maximum volumes were nearly constant suggest that for both regimes, perturbations of similar wavelengths may have been responsible for the detachment of bubbles (Lamb, 1932; Foster, 1971). Photographs (Figs 7 and 8) show that the projected cavities collapsed non-uniformly and more rapidly from the sides in the detachment phase. Cavity elongation in the cylindrical configuration continued while a constriction formed.

The cavity evolved to produce tapered jets (with aspect ratios of between 1 and 1.5) from the tip of which tiny vapor bubbles were released in the transition zone between an unstable jet and a continuous two-phase jet. This suggests that the capillary number $(\mu U/\sigma)$ for the system was between 0.25 and 0.33 at a steam supply rate of around 6.7 $g\,s^{-1}$ (Taylor, 1934; Rumscheidt and Mason, 1961). The relative velocity between the liquid and the vapor at the interface may consequently be estimated using the properties of water at 100°C [$\sigma = 5.89\ (10^{-2})\,N\,m^{-1}$; $\mu = 2.79\ (10^{-4})$ Pa · s] to be of the order of 30–35 $m\,s^{-1}$. This is considerably lower than the vapor velocity of 342 $m\,s^{-1}$ through the orifice although it is an order of magnitude higher than that presented in Fig. 3b. In this regime, a higher fraction of vapor would be condensed after bubbles had been pinched from the jets than at lower steam rates.

For vapor supply rates of 1.45 $g\,s^{-1}$ (discrete bubble regime) and 3.41 $g\,s^{-1}$ (unstable jet), convective heat transfer coefficients were evaluated versus time for cavity growth cycles using eqs (1) and (2) and the data in Figs 4 and 5. The results are presented in Fig. 10. At 1.45 $g\,s^{-1}$ steam supply rate, the heat transfer coefficients were higher than 2.0 $(10^{6})\,W\,m^{-2}\,K^{-1}$ while the vapor–liquid interface resided in the pore of the nozzle and was in ascent. Immediately after the interface emerged, the coefficient dropped by about 50% as the interface was exposed to and in relative motion to the liquid pool. The larger scale oscillations at the interface decreased

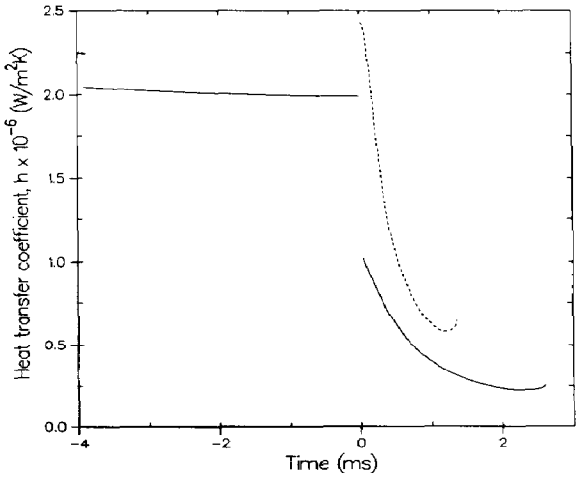

Fig. 10. Heat transfer coefficients during the growth of vapor cavities at steam supply rates of 1.45 $g\,s^{-1}$ (solid lines) and 3.41 $g\,s^{-1}$ (dashed line). The instant when the interface emerged from the orifice was set at time zero. Only for the ascent phase of the interface were the coefficients calculated. While within the nozzle pore, the interface oscillated rapidly and the coefficients were high. A primary bubble was detached after $\simeq$ 2.6 ms after emergence above the orifice at a steam rate of 1.45 $g\,s^{-1}$, and after $\simeq$ 1.3 ms at 3.41 $g\,s^{-1}$.

but the smaller scale interfacial turbulence appeared undisturbed or even enhanced during the emergence. As the cavity expanded, the coefficient continued to decrease to about 2.4 (10^5) W m^{-2} K^{-1} just before bubble release. Coefficients at the start of interface displacement were higher by an order of magnitude than the time-averaged values previously reported for heat transfer coefficients of 7.6 (10^4)–1.74 (10^5) W m^{-2} K^{-1} by Bankoff and Mason (1962). In their experiments, a downward water jet was made to impinge on vapor cavities and bubbles formed at 0.5 and 1.73 mm diameter nozzles. The liquid current apparently dampened the interfacial turbulence and modified the contour which bubbles would naturally have assumed. The bubbles may have been flattened to ellipsoidal shapes with higher eccentricities much earlier in the growth phase than would otherwise have been achieved. As the data in Fig. 10 show, the average surface heat transfer coefficient was lowest for the ellipsoidal configurations. The range for heat transfer coefficients estimated in this study is also an order of magnitude higher than the 7.9 (10^4)–1.14 (10^5) W m^{-2} K^{-1} range reported by Grassman and Wyss (1962). The difference may be attributed to the low subcooling (0.4–2.8°C) the authors employed and the small diameter of the orifice (1.2 mm). A heat transfer coefficient of 1.2 (10^6) W m^{-2} K^{-1} has been calculated for a steam supply rate of 1.7 g s^{-1} which is within the transition zone for formation of discrete bubble and unstable jet regimes. This zone, as previously described (Fig. 6), would correspond to a pseudo-stationary state and the plume formed would be nearly pure.

In the unstable jet regime, vapor did not retract into the nozzle pore. Hence a discontinuity in the heat transfer coefficient with time was neither anticipated nor observed. The heat transfer coefficients at the beginning of the growth cycle were high, i.e. $\simeq$ 2.4 (10^6) W m^{-2} K^{-1}, and then decreased to about 25% of the starting value when a bubble was to be released. The pattern of change suggests that the displacement of the interface has a dampening effect on the local turbulence near the vapor–liquid boundary.

CONCLUSIONS

Data from high speed photography and frequency measurements have been used to establish that steam injected into water with a subcooling of 80–100°C formed bubbles from cavities in three regimes as vapor rate was increased. In the transition between discrete bubble release and unstable jets regimes, the vapor–liquid interface was nearly stationary and flat for considerable periods and latent energy was convected away from the interface to form nearly pure buoyant plumes. The second transition between unstable and continuous two-phase jet regimes involves oscillations of a prolate ellipsoidal interface between axisymmetric jets which released large bubbles and tapered sinuous jets which exhibited "tip streaming". Convective heat transfer coefficients were calculated for the growth phase of the interfaces in the single bubble and unstable jet regimes. While the vapor–liquid boundaries were confined within the pore of the nozzle in the discrete bubble regime, heat transfer coefficients were higher than 2.0 (10^6) W m^{-2} K^{-1}. The value dropped almost discontinuously after the interface emerged above the orifice and further decreased to about 10% of the above value while a cavity grew until bubble detachment. The coefficient in the unstable jet regime was initially about 2.4 (10^6) W m^{-2} K^{-1} and the magnitude decreased by about 75% during an interval of about 1.4 ms while the vapor cavity expanded and changed shape to release a bubble. The heat transfer coefficients determined are an order of magnitude greater than were reported previously by Bankoff and Mason (1962) and Grassman and Wyss (1962). The differences may be attributed to the larger orifice and higher subcooling used in the current study. The volumes of the cavities and the time for growth were much smaller than for the air–water system at similar bubbling regimes.

Acknowledgements—The first author acknowledges funding support from NSERC (Canada) and AOSTRA. Darren Koon's expert assistance with data processing is much appreciated.

NOTATION

A	area of vapor–liquid interface, m^2
C_p	thermal capacity or specific heat, J kg^{-1} K^{-1}
d	diameter, m
g	acceleration of gravity, m s^{-2}
h	convective heat transfer coefficient, W m^{-2} K^{-1}
H_v	enthalpy of vapor, J kg^{-1}
k	thermal conductivity, W m^{-1} K^{-1}
$\dot{m}$	vapor rate through nozzle, kg s^{-1}
P	vapor pressure, Pa
Q	volumetric flow rate of vapor, m^3 s^{-1}
Q_k	"kinematic" heat flux, mK s^{-1}
r_0	radius of nozzle pore
t	time, s
T	temperature, °C
u, U	velocity, m s^{-1}
V	volume of cavity above the nozzle or of bubble, m^3
$\dot{V}$	rate of increase in cavity volume, m^3 s^{-1}

Greek symbols

α	coefficient of volume expansion, K^{-1}
Δ	change from vapor to liquid
κ	thermal diffusivity $(k/\rho c_p)$, m^2 s^{-1}
Λ	mass rate [eq. (2)], kg s^{-1}
μ	viscosity of liquid, Pa·s
ν	kinematic viscosity (μ/ρ), m^2 s^{-1}
σ	surface tension of vapor–liquid interface, N m^{-1}
ρ	density, kg m^{-3}
ϕ	parameter for estimating bubble volume

Subscripts

b	value for bulk liquid or for bubble
S or sat	for saturated steam
v	for vapor
0	for vapor through nozzle or for nozzle
l	for liquid

REFERENCES

Abramovich, G. N., 1963, *The Theory of Turbulent Jets.* M.I.T. Press, Cambridge, MA.

Bankoff, S. G. and Mason, J. P., 1962, Heat transfer from the surface of a steam bubble in turbulent subcooled liquid stream. *A.I.Ch.E. J.* **8**, 30–33.

Benjamin, T. B. and Ellis, A. T., 1966, The collapse of cavitation bubbles and the pressures thereby produced against solid boundaries. *Phil. Trans. R. Soc.* **A260**, 221–240.

Chandrasekhar, S., 1961, *Hydrodynamic and Hydromagnetic Stability.* Clarendon Press, Oxford.

Chen, C. J. and Rodi, W., 1980, *Vertical Turbulent Buoyant Jets. A Review of Experimental Data.* Pergamon Press, Oxford.

Clift, R., Grace, J. R. and Weber, M. E., 1978, *Bubbles, Drops and Particles.* Academic Press, New York.

Davidson, J. F. and Schüler, B. O. G., 1960a, Bubble formation at an orifice in a viscous liquid. *Trans. Inst. Chem. Engrs* **38**, 144–154.

Davidson, J. F. and Schüler, B. O. G., 1960b, Bubble formation at an orifice in an inviscid liquid. *Trans. Inst. Chem. Engrs* **38**, 144–154.

Foster, T. D., 1971, Intermittent convection. *Geophys. Fluid Dyn.* **2**, 201–217.

Gardner, F. H., Nutt, C. N. and Mohtadi, M. F., 1955, Pulsation and mass transfer of pendant liquid droplets. *Nature* **175**, 603–604.

Grassman, P. and Wyss, E., 1962, Bestimmung von Wärme- und Stoffübergangszahlen zwischen Dampfblase und flüssigkeit. *Chemie-Ing.-Techn.* **34**, 755–759.

Howard, L. N., 1963, Heat transport by turbulent convection. *J. Fluid Mech.* **17**, 405–432.

Jeje, A. and Ross, B., 1988, The temperature field near a nozzle and the dynamics of saturated steam bubbles in subcooled water at low steady vapor supply rates. *Chem. Engng Sci.* **43**, 2817–2831.

Kobus, H. E., 1968, Analysis of flow induced by air–bubble systems. *Proc. 3rd. int. Conf., BOSS*, Vol. 1, pp. 1016–1031.

Koschmieder, E. L. and Pallas, S. G., 1974, Heat transfer through a shallow horizontal convecting fluid layer. *Int. J. Heat Mass Transfer* **17**, 991–1002.

Krishnamurti, R., 1970, On the transition to turbulent convection. Parts 1 and 2. *J. Fluid Mech.* **42**, 293–307 and 311–320.

Kumar, R. and Kuloor, N. R., 1970, The formation of bubbles and drops. *Adv. Chem. Engng* **8**, 256–368.

Lamb, H., 1932, *Hydrodynamics*, 6th edn. Dover, New York.

Lauterborn, W. and Bolle, H., 1975, Experimental investigations of cavitation-bubble collapse in the neighbourhood of a solid boundary, *J. Fluid Mech.* **72**, 391–399.

Levich, V. G., 1962, *Physiochemical Hydrodynamics.* Prentice-Hall, Englewood Cliffs, NJ.

Milgram, J. H., 1963, Mean flow in round bubble plumes. *J. Fluid Mech.* **133**, 345–376.

Mollendorf, J. C., Arif, H. and Ajiniran, E. B., 1984, Developing flow and transport above a suddenly heated horizontal surface in water. *Int. J. Heat Mass Transfer* **27**, 273–289.

Pinczewski, W. V., 1981, The formation of growth of bubbles at submerged orifices. *Chem. Engng Sci.* **36**, 405–411.

Plesset, M. S. and Chapman, R. B., 1971, Collapse of an initially spherical vapor cavity in the neighbourhood of a solid boundary. *J. Fluid Mech.* **47**, 283–290.

Plesset, M. S. and Prosperetti, A. 1977, Bubble dynamics and cavitation. *Ann. Rev. Fluid Mech.* **9**, 145–185.

Rallison, J. M., 1984, The deformation of small viscous drops and bubbles in shear flow. *Ann. Rev. Fluid Mech.* **16**, 45–66.

Richards, J. M., 1965, Puff motions in unstratified surroundings. *J. Fluid Mech.* **21**, 97–106.

Rumscheidt, R. D. and Mason, S. G., 1961, Particle motions in sheared suspensions. xii. Deformation and burst of fluid drops in shear and hyperbolic flow. *J. Colloid Sci.* **16**, 238–261.

Shaw, R., 1984, *The Dripping Faucet as a Model Chaotic System.* Aerial Press, Santa Cruz, CA.

Sideman, S., 1966, Direct contact heat transfer between immiscible liquids. *Adv. Chem. Engng* **6**, 207–286.

Silberman, E., 1957, Production of bubbles by the disintegration of gas jets in liquid. *Proc. 5th Midwestern Conf. Fluid Mech.*, Michigan, pp. 263–285.

Tan, R. B. H. and Harris, J. J., 1986, A model for non-spherical bubble growth at a single orifice. *Chem. Engng Sci.* **41**, 3175–3182.

Taylor, G. I., 1934, The formation of emulsions in definable fields of flow. *Proc. R. Soc. Ser. A* **146**, 501–523.

Turner, J. S., 1973, *Buoyancy Effects in Fluids.* Cambridge University Press, U.K.

van Krevelen, D. W. and Hoftijzer, P. J., 1950, Studies of gas-bubbles formation. *Chem. Engng Prog.* **46**, 29–35.

Wegener, P. P. and Parlange, J.-Y., 1973, Spherical-cap bubbles. *Ann. Rev. Fluid Mech.* **5**, 79–100.

Zauner, E., 1985, Visualization of the viscous flow induced by a round jet. *J. Fluid Mech.* **154**, 111–119.